# BEST AVAILABLE IMAGES

Defective images within this document are accurate representations of the original documents submitted by the applicant.

Defects in the images may include (but are not limited to):

- BLACK BORDERS
- TEXT CUT OFF AT TOP, BOTTOM OR SIDES
- FADED TEXT
- ILLEGIBLE TEXT
- SKEWED/SLANTED IMAGES
- COLORED PHOTOS
- BLACK OR VERY BLACK AND WHITE DARK PHOTOS
- GRAY SCALE DOCUMENTS

## IMAGES ARE BEST AVAILABLE COPY.

**As rescanning documents *will not* correct images, please do not report the images to the Image Problem Mailbox.**

...l. Chem. 1997, 69, 2035–2042

XP 000696542

# ...V Laser Machined P...lymer Substrat...s f...r th...)ev...l...pm...nt of Micr...diagnostic Syst...ms

**...atthew A. R...berts, Joël S. Rossier, Paul Bercier, and Hubert Girault***

...boratoire d'Electrochimie (ICP), Département de Chimie, Ecole Polytechnique Federale de Lausanne, ...015-Ecublens, Switzerland

...is report describes a UV laser photoablation method ...r the production of miniaturized liquid-handling systems ...n polymer substrate chips. The fabrication of fluid ...annel and reservoir networks is accomplished by firing ...00 mJ pulses from an UV excimer laser at substrates ...oving in predefined computer-controlled patterns. This ...ethod was used for producing channels in polystyrene, ...olycarbonate, cellulose acetate, and poly(ethylene tere...hthalate). Efficient sealing of the resulting photoablated ...olymer channels was accomplished using a low-cost film ...umination technique. After fabrication, the ablated struc...res were observed to be well defined, i.e., possessing ...igh aspect ratios, as seen by light, scanning electron, and ...omic force microscopy. Relative to the original polymer ...amples, photoablated surfaces showed an increase in ...eir hydrophilicity and rugosity as a group, yet differ...nces were noted between the polymers studied. These ...urface characteristics demonstrate the capability of ...enerating electroosmotic flow in the cathodic direction, ...hich is characterized here as a function of applied ...lectric field, pH, and ionic strength of common electro...horetic buffer systems. These results show a correlation ...etween the ablative changes in surface conditions and ...he resulting electroosmotic flow. The effect of protein ...oatings on ablated surfaces is also demonstrated to ...ignificantly dampen the electroosmotic flow for all poly...ners. All of these results are discussed in terms of ...eveloping liquid-handling capability, which is an es...ential part of many μ-TAS and chemical diagnostic ...ystems.

In this article, we present the development and characterization ...f microfabricated fluid channels in polymer substrates using the ...echnique of UV excimer laser photoablation. These structures, ...with their ability to generate electroosmotic flow, should find ...application in conventional as well as miniaturized capillary ...electrophoresis (CE) instrumentation as liquid-handling platforms. ...Using this method, microchannel structures are easy to fabricate ...on inexpensive polymer substrates, and, therefore, there is also ...potential for development of disposable diagnostic systems.

Capillary electrophoretic methods have enjoyed increasing ...popularity due to the observed high separation efficiencies, peak ...efficiency, and wide dynamic ranges of molecular weights that ...may be analyzed.[1] Recently, there has also been intense activity ...in the miniaturization of chemical instrumentation. Efforts have ...been made to reduce whole laboratory systems onto microchip ...substrates, often utilizing CE as the principal analytical technique.[2] These systems have been termed microscale total analytical systems (μ-TAS).[3] Several bioanalytical applications have been demonstrated in the recent literature with apparently very promising capabilities.[4–7]

Most μ-TAS devices to date have been produced photolithographically on substrates such as glass, quartz, and silicon. These substrates have an abundance of charged silanol groups and are thus capable of generating electroosmotic flow. In the case of these miniaturized electrophoretic systems, electroosmotic flow is considered advantageous, in that it can be used for various liquid-handling operations and is considered essential to the operation of many on-chip methods of analysis.[4]

The miniaturization of mechanical components for liquid handling, such as pumps and valves, is technically problematic, which is another factor spurring the development of microfabricated CE (herein termed μ-CE) systems.[4] Electroosmotic flow control provides many advantages for microfabricated chemical analysis platforms due to the ease of fabrication (only two electrodes are required), good reproducibility, and short analysis times associated with its use.[2,3,10] Resulting systems in many ways resemble flow injection analysis (FIA) with their ability to deliver sample plugs to precise locations in whole networks of capillaries. Furthermore, the connection of multiple capillaries into networks is easily accomplished in these systems, with a minimum of dead volume, something which has proven more difficult to do in conventional CE.[9]

Laboratories have recently demonstrated the potential of μ-CE systems of interconnected capillaries for the separation of oligonucleotides,[2] amino acids,[11] and fluorescent dyes.[3,10] Maximum separation efficiencies, limited only by diffusion, injection, and detection, have been achieved using microfabricated systems.[12] Immunoassay has also been recently demonstrated in a micro-

(1) Tavares, M. F. M.; Mcquffin, V. L. *Anal. Chem.* **1995**, *67*, 3687–3696.

(2) Arquint, P.; Koudelka-Hep, M.; van der Schoot, B.; van der Wal, P.; de Rooij, N. F. *Clin. Chem.* **1994**, *40*, 1805–1809.

(3) Manz, A.; Graber, N.; Widmer, H. M. *Sens. Actuators B* **1990**, 244.

(4) Murakami, Y.; Takeuchi, T.; Yokoyama, K.; Tamiya, E.; Karube, I. *Anal. Chem.* **1993**, *65*, 2731–2735.

(5) Jacobson, S. C.; Koutny, L. B.; Hergenroder, R.; Moore, A. W.; Ramsey, J. M. *Anal. Chem.* **1994**, *66*, 3472–3476.

(6) Koutny, L. B.; Schmalzing, D.; Taylor, T. A.; Fuchs, M. *Anal. Chem.* **1996**, *68*, 18–22.

(7) Effenhauser, C. S.; Manz, A. *Am. Lab.* **1994**, September, 15–18.

(8) Seiler, K.; Harrison, D. J.; Manz, A. *Anal. Chem.* **1993**, *65*, 1481–1488.

(9) Burggraf, N.; Manz, A.; Verpoorte, E.; Effenhauser, C. S.; Widmer, H. M.; de Rooij, N. F. *Sens. Actuators B* **1994**, *103*–110.

(10) Jacobson, S.; Hergenroder, R.; Koutny, L. B.; Ramsey, J. M. *Anal. Chem.* **1994**, *66*, 1114–1118.

(11) Harrison, D. J.; Fluri, K.; Seiler, K.; Fan, Z.; Effenhauser, C. S.; Manz, A. *Science* **1993**, *261*, 895–897.

(12) Effenhauser, C. S.; Manz, A.; Widmer, H. M. *Anal. Chem.* **1993**, *65*, 2637–2642.

S0003-2700(96)01038-4 CCC: $14.00 

machined CE device by Koutny et al. [illegible]rtisol was determined in serum using a competitive immunoassay that was subsequently quantitated using $\mu$-CE. Separation of the immunoassay components was accomplished in under 30 s, with a resolution of 400 theoretical plates/s.

The standard process for generating $\mu$-TAS devices involves the generation of the desired pattern on a photomask, through which a photoresist-coated crystalline surface is exposed to light. Solubilized photoresist is then removed and the resulting pattern anisotropically etched with hydrofluoric acid. All steps must be carried out under clean room conditions, which adds considerable overhead cost to production of $\mu$-TAS systems. Etched capillaries are then generally sealed by some bonding method to a glass cover. The bonding techniques, which normally involve thermal bonding,[7,8,11,12] can also be labor and technology intensive, requiring temperatures of up to 1000 °C. If one wishes to explore the site-specific deposition or preapplication of affinity matrices/biological receptors within capillary networks, then these fabrication techniques may be limited.

This article will describe an alternative method for creating such systems by fabrication of photoablated polymer capillaries and their subsequent sealing using an easy-to-use, low-temperature lamination process. Furthermore, due to the nature of the photoablative process, structures are self-cleaning during fabrication and, therefore, do not require clean room conditions. This work presents a description of the generation of electroosmotic flow on photoablated polymer substrates for the first time. All flow operations in these microchannels are carried out with the application of an external electrical field in order to direct the resulting electroosmotic flow toward liquid reservoirs, which should be suitable for liquid handling in $\mu$-TAS systems. The resulting devices maintain the beneficial liquid-handling capabilities, based on electroosmotic flow, seen with devices photolithographically defined in glass, quartz, or silicon. Polymer substrates also offer several distinct advantages, which include but are not limited to a single, easy-to-perform process for the generation of structural components (capillaries, fluid reservoirs, sample injectors, etc.), high geometrical aspect ratios, nearly vertical side walls, and a low-temperature sealing method compatible with sensitive biological agents, allowing easy deposition or conjugation prior to sealing of devices.

Photoablated microchannels are described here according to their ability to generate electroosmotic flow and their potential to be used in $\mu$-TAS liquid-handling operations. For the purposes of this study, only simple line and circular patterns were used; however, it should be stressed that more complicated channel geometry can be fabricated using UV laser photoablation. The work presented here describes a method of production and outlines for the first time the liquid-handling capabilities of the resulting photoablated polymer structures.

## EXPERIMENTAL SECTION

**Reagents.** Polycarbonate sheets (1 mm thick) were obtained from Rohm (GmbH) under the trade name Makrolon. Polystyrene sheets (1.2 mm thick) were obtained from Sigma Chemical Co. (St. Louis, MO). Poly(ethylene terephthalate) sheets (100 $\mu$m thick) were obtained from ICI (UK) under the name Melinex (grade S). Cellulose acetate sheets (100 $\mu$m thick) were obtained under the trade name Tartan. Poly(ethylene terephthalate), 35 $\mu$m thick with a 5 $\mu$m thick adhesive polyethylene adhesive on one side, was used as the laminating film (PET/PE) for all photoablated structures and was obtained from Morane (Oxon, UK). Bovine serum albumin (BSA) was obtained from Sigma. Citrate buffer, pH 4.0 (56 mM citrate/68 mM sodium hydroxide/44 mM sodium chloride), phosphate buffer, pH 7.0 (26 mM potassium dihydrogen phosphate/41 mM disodium phosphate), and borate buffer, pH 10.0 (13 mM sodium tetraborate/18 mM sodium hydroxide), were obtained from Fluka (Buchs, Switzerland). Eosin B was purchased from Aldrich (Milwaukee, WI).

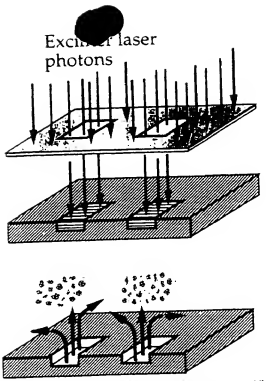


**Figure 1.** UV laser micromachining process. UV excimer laser pulse rapidly breaks chemical bonds within a restricted volume to cause a miniexplosion and ejection of ablated material.

**Fabrication of UV Laser Photoablated Fluid-Handling Microchannels.** Many commercially available polymers are known to photoablate upon interaction with UV laser radiation. These have been reviewed,[13] but they include polycarbonate, poly(methyl methacrylate) (PMMA), polystyrene, nitrocellulose, poly(ethylene terephthalate) (PET or Melinex), and poly(tetrafluoroethylene) (Teflon). The photoablation process involves absorption of short-duration laser pulses in the UV region with concomitant electronic transitions from the ground singlet state to the first excited singlet states and bond breaking within the long-chain polymer molecules.[13] Finally, there is a resulting shock wave and the ejection of decomposed polymer fragments, leaving a photoablated cavity as depicted in Figure 1.[14] The ejected material is made up of gas ($C_2$, $CO_2$, CO), polymer molecules, and small particulate matter. Due to the "ejection by pressure" process, each successive pulse of the laser functions to clean away any debris that might have accumulated in the ablative region. Therefore, structure quality can be maintained under non-clean room conditions.

The laser energy can be specifically patterned using a mask with the subsequent generation of microcavities and channels in various geometry. The resulting structures are generally characterized as having little thermal damage, straight vertical walls,

(13) Srinivasan, R.; Braren, B. *Chem. Rev.* **1989**, *89*, 1303−1316.
(14) Reyna, L. G.; Sobehart, J. R. *J. Appl. Phys.* **1994**, *76*, 4367−4371.

and well-defined depth.[10,13] For this investigation, it was necessary only to use simple line-and-hole mask geometry. For the simplest linear embodiments used here, a 10 mm × 0.4 mm mask was mechanically fabricated in copper foil. For reservoir fabrication, a 5 mm diameter circular mask was machine drilled in a 5 mm thick steel plate. An excimer laser (Lambda Physik LPX 205 i, Goettingen, GmbH) was used to project UV laser radiation (200 mJ/pulse at 193 nm, pulse rate = 10–50 Hz) through these masks, through a 10:1 telescopic objective, and then onto various polymer substrates. Therefore, each laser pulse will produce an ablated cavity with a cross-sectional area of 1 mm × 0.04 mm when using the line mask and a 0.5 mm diameter hole when using the circular mask.

Prior to laser machining, all substrate samples were cleaned by a standard procedure. This involved initially rinsing them with distilled water and then bathing them in a 0.1 M NaOH solution for 30 min. Samples were then rerinsed with distilled water, dried under pressurized air, and then mounted onto an *X,Y* machining stage.

During the pulsed ablation process, the substrate was moved horizontally with an *X,Y* stepper motor between 0.05 and 0.2 mm/s in order to generate linear microchannels with final dimensions of 23 mm × 0.04 mm of a specified depth. The speed of substrate movement and the laser pulse frequency were used to control the total number of pulses impinging on any given substrate area, therefore, the resulting microchannel depth. For all of the electroosmotic flow data presented, channels were fabricated by pulsing the laser at 50 Hz and moving the substrate at 0.2 mm/s. This corresponds to 250 pulses/mm and was observed to produce channels of approximately 37 $\mu$m in depth.

**Sealing and Access to Photoablated Microchannels.** Prior to sealing, ablated microchannels were cleaned under a jet of compressed air. Sealing was accomplished by thermal lamination with a PET/PE film (35 mm thick) at 125 °C using a standard industrial lamination apparatus (Morane Senator (pneumatic control), Oxon, U.K). The simplicity of sealing photoablated polymer devices should be firmly emphasized here as another distinct advantage of using UV laser photoablative micromachining for the construction of polymer-based $\mu$-CE chemical analysis systems. The low temperature and rapid sealing (< 2 s exposure to raised temperatures) could even allow the predeposition of sensitive biological reagents, which will subsequently retain their desired activity after device fabrication.

Fluid access to ablated microchannels was achieved by two principal methods. In the first case, for substrates greater than 200 $\mu$m thick, such as our polycarbonate and polystyrene samples, lines were first fabricated, as described above, and then completely sealed off with the PET/PE laminate. Subsequently, circular holes were laser ablated over the ends of microchannels using 500, 200 mJ pulses through a 5 mm diameter mask. An example of these access reservoirs is pictured in Figure 2a.

In the second case, for very thin substrates (< 200 $\mu$m), the laser was directed to fire 500, 200 mJ pulses through a 5 mm diameter mask at the beginning and end of a channel. With the cellulose acetate and PET samples used here, this was sufficient to create an opening completely through the substrate film. One face of these structures was then sealed off with the PET/PE laminate. After this lamination procedure, microchannels could be accessed through the hole openings in the substrate from the opposite side of the PET film with the channel lying at the bottom level of the access reservoirs. An example of reservoirs formed using this method is shown in Figure 2b. This method is preferred since only one ablative step is required, and no alignment of a second mask pattern is necessary after removal of the sample from the *X,Y* stage.

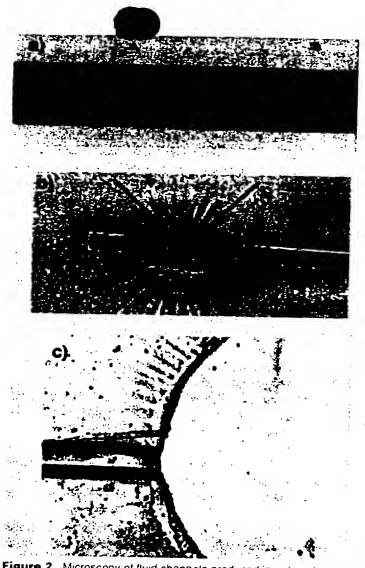


**Figure 2.** Microscopy of fluid channels produced in polycarbonate by UV laser micromachining. (a) Dye-filled capillary demonstrating efficient sealing with a low-temperature (125 °C) PET/PE lamination process. (b) Fluid access reservoir formed through the PET PE sealing layer by applying a 500 pulse, 50 Hz burst of 200 mJ UV laser energy after lamination (method 1). (c) Fluid access reservoir formed through a 100 $\mu$m thick cellulose acetate substrate by applying a 500 pulse, 50 Hz burst of 200 mJ UV laser energy prior to lamination (method 2).

After fabrication by either method, small microwells (40–50 nL capacity) were made from commercially available food tubing and attached over reservoir openings using a chemically inert epoxy.

**Characterization of Fluid Handling in Sealed Capillaries.** Sealed capillaries were filled with a peristaltic pump, which was connected to the fluid reservoirs via the food tubing reservoirs. It should be noted that a good lamination seal was maintained even while pumping by external pressure at flow rates up to 40 nL/min (internal microchannel volume = 36 nL). Higher flow rates were not tested, so the upper pressure limits of these systems is not known presently.

(13) Niino, H.; Yabe, A. *Appl. Surf. Sci.* **1993**, *69*, 1–5.

The detection of leaks or lamina[redacted]res could be easily visualized by adding 10 mM Eosin B to a phosphate buffer filling solution. No leaks were detected during capillary filling or external pumping, indicating a strong seal when using the PET/PE lamination at 125 °C. An example of a dye-filled microchannel with no leaks is demonstrated in Figure 2c.

After filling, platinum electrodes were inserted in either reservoir, and an electric field was applied using a Landis & Gyr high-tension power supply. Electroosmotic flow was monitored using the technique of Huang et al.[16] Briefly, this method involves filling ablated channels by capillary action with a buffer of a given electrolyte concentration. Subsequently, the inlet reservoir solution is aspirated and replaced with a buffer of somewhat lower electrolyte concentration. Unless stated otherwise, the total salt strength of the initial fill buffer (phosphate buffer, pH 7.0, Fluka) was 12 mM. An electric potential ($E$) is then applied across the capillary, and the current is monitored. The electroosmotic flow will direct liquid through the capillary, from anode to cathode. As the lower strength buffer moves through the capillary, the resistance will increase and the current will decrease. At some time ($t$), the capillary will be completely filled with the second buffer, and the current will be constant.

The electroosmotic flow velocity ($v_{EOF}$) can then be calculated as the length of the capillary ($L$) divided by $t$, and the electrophoretic mobility ($\mu_{EOF}$) is $\mu_{EOF} = v_{EOF}/E$. The $v_{EOF}$ can also be used to calculate the $\zeta$ potential for each surface under our experimental conditions from the equation given by Tavares and McGuffin:[2] $v_{EOF} = -\epsilon_0\epsilon\zeta E/\eta$, where $\epsilon_0$ is the permittivity of free space, $\epsilon$ is the dielectric constant, $\zeta$ is the potential, and $\eta$ is the viscosity of the buffer solution.

The EOF was determined by this technique for both untreated and BSA-coated microchannels. To prepare BSA-coated channels, a phosphate-buffered solution (pH 7.0) of BSA (10 mg/mL) was pumped through channels created as above in polystyrene, polycarbonate, cellulose acetate, and poly(ethylene terephthalate). The pump was then turned off and the solution allowed to contact the photoablated channel for 30 min at room temperature. After this incubation period, the inlet and outlet reservoir solutions were replaced with the standard phosphate buffer. A voltage of 250 V·cm$^{-1}$ was then applied to the channels for 10 min in order to wash them by electroosmotic pumping. The concentration of protein in both the inlet and outlet reservoirs was then monitored by conventional capillary electrophoresis (BioFocus 3000, Bio-Rad, Hercules, CA), which had an absolute detection limit of 10 ng for BSA.

The electrophoresis of a test dye was observed between 0 and 500 V·cm$^{-1}$. A high concentration (10 mM) of Eosin B was added to a fluid reservoir and then injected onto a microchannel with electroosmotic flow using an applied electric field of 500 V·cm$^{-1}$ for 3 s. The fluid reservoir was then aspirated and the fluid replaced with 12 mM phosphate running buffer. The field was subsequently reapplied at various levels, and the migration velocity of the Eosin B zone was recorded using a CCD camera mounted directly on a light microscope and connected to a video recorder.

The electroosmotic flow was measured as a function of the buffer ionic strength. This was done by diluting a standard phosphate buffer, pH 7.0, and then rechecking that the pH was within 0.1 unit. As this buffer system is a mixed cation system ($3.15Na^+$:$1K^+$), it is more easily listed, simply by the overall salt concentration ($C$) [redacted]as varied from 6 to 100 mM. The $v_{EOF}$ was observed by t[redacted]rent monitoring technique as previously described.

Citrate, phosphate, and borate buffer systems of pH 4, 7, and 10 were used to characterize the electroosmotic flow response of the photoablated surface to changes in pH/buffer types. All buffers were adjusted to equal ionic strength, and then electroosmotic flow was measured as described earlier.

***Safety Considerations:*** UV laser energy is dangerous and standard laser laboratory safety equipment should be used, including protective eyewear.

## RESULTS AND DISCUSSION

**Characterization of Photoablated Cavities.** The relationship between the number of laser pulses, laser frequency, and the resulting microchannel depth was studied using SEM. Samples were generated using a static substrate and a photomask of the dimensions previously described. Two hundred millijoule UV laser pulses were focused on a polycarbonate surface, and 0−1000 pulses were fired at 10, 20, and 50 Hz. Samples were then analyzed by scanning electron microscopy (SEM). The channel depth could be determined in this manner using a high tilt angle (60 °C) and subsequent measurements of an exposed depth profile. The channel depth was found to be essentially linear and did not vary with frequency according to the following relationship: depth ($\mu$m) = 0.148$N$, where $N$ is the number of laser pulses (200 mJ/pulse).

It should be noted that the geometries of cavities produced by this technique vary little over their entire depth profile, i.e., producing very straight side walls, as seen by AFM (not shown) and SEM. A profile of a 500 pulse microchannel is shown in Figure 3a. It can be seen that all angles are relatively sharp and the channel side walls are essentially vertical for channel depths of at least 75 $\mu$m.

The cross-sectional profile of photoablated microchannels was also examined by SEM, as shown in Figure 3b. It can be seen that the interface between the PET/PE laminate and a photoablated channel is well defined across a 190 mn wide gap and shows good adherence to the corners. The lamination profile, just above the channel, does not show any deformation into the gap, which is important for the reproducible manipulation of fluids, even over a 190 $\mu$m wide gap.

For deeper channels (>20 $\mu$m), the rugosity is more pronounced on the bottom surface and is characterized in Figure 4 and Table 1. The rugosity of unablated polymer substrates was observed as only a 0.01 $\mu$m depth variation across a 70 × 70 $\mu$m$^2$ cross section. Photoablated polycarbonate and polystyrene surfaces appear to have a small undulating rugosity and are very similar to one another, with variations of the average depth of 0.13 $\mu$m. In contrast, it can be seen that cellulose acetate and poly(ethylene terephthalate) surfaces show very pronounced rugged projections on the submicrometer scale and differ in the overall magnitude of this effect. Photoablated cellulose acetate showed an increase in rugosity (0.27 $\mu$m) relative to those just mentioned; however, poly(ethylene terephthalate) showed the largest increase, with an overall depth variation of 0.40 $\mu$m.

The rugosity of photoablated surfaces will certainly increase the adsorption of many substances and, therefore, may interfere with high-efficiency separations. However, it should be noted that even these more rugged surfaces display features approximately 2 orders of magnitude less than the overall channel depth, which

(16) Huang, X.; Gordon, M.; Zare, R. N. *Anal. Chem.* **1988**, *60*, 1837−1838.

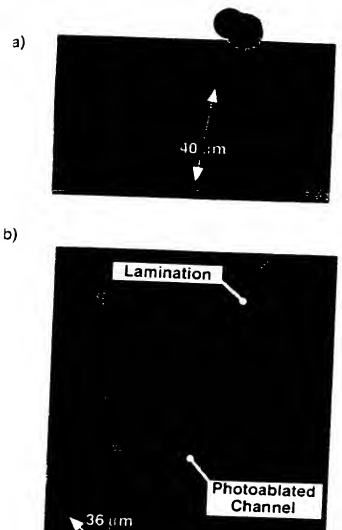


**Figure 3.** Profiles of photoablated polymer microchannels. (a) SEM image of photoablated microchannel (500× magnification, 60° tilt angle). (b) Microchannel entrance between the polycarbonate substrate and PET/PE laminate. SEM image (800× magnification) of channel showing straight side walls and PET/PE lamination interface (bottom).

should not drastically affect the hydrodynamic properties of the bulk solution. This will affect the surface area of the microchannel, which, in turn, will affect the electroosmotic flow, which is very sensitive to both the physical and chemical changes on the surface. From the perspective of developing microfabricated diagnostic assays, the increased surface area, seen particularly with photoablated poly(ethylene terephthalate), could be very useful for the deposition of receptor and ligand zones. Since the adsorption will be directly related to the surface area of the assay format, much more concentrated regions of immobilized biomolecules may be obtained.

**Electroosmotic Flow and Electrophoresis on Various Photoablated Polymer Surfaces.** Four polymer substrates, polystyrene, polycarbonate, cellulose acetate, and poly(ethylene terephthalate), were studied after photoablation. When this fabrication method is performed under an ambient atmosphere, there exists the possibility for incorporation of either oxygen or nitrogen into the structure of decomposition products. The resulting structures may then give rise to amino, hydroxyl, carboxylic, and phenolic functional groups.[15,17,18] Studies of the exact chemical nature of functionalized surfaces were beyond the scope of these fluid-handling experiments; however, the resulting electroosmotic flow within structures formed from the four polymers was used to obtain information concerning the charged nature of the ablated surfaces. In all cases, electroosmotic flow could be generated in the direction of the cathode when an external electric field was applied. This directly implies a net negative surface charge, which is believed to be the result of chemical functionalities generated due to the incorporation of oxygen during the photoablative process.

Previous studies have noted differential chemical changes between the ablated substrate and ablatively ejected particles. The ablated substrate surface has been examined by others using XPS and SIMS techniques, which has generally indicated an increased carbon/oxygen ratio when compared with that of the original substrate.[19] In general, this corresponds to a less charged, more hydrophobic surface; however, oxygen incorporation and an increased charge have been noted for the ablatively ejected fragments created during fabrication.[19,20] These heated particles are often redeposited onto the surrounding substrate, thereby creating charged hydrophilized surfaces.

It is important to note that the studies presented here use the technique of laser drawing, where the substrate is moved under a repeatedly fired UV excimer laser. Therefore, as structure is created and then moved out of the path of the laser beam, deposition of ejected molecules becomes possible. The ejected particles may then form a path just behind the laser throughout the pattern that is under fabrication. Only structures ablated without substrate movement will have the higher carbon/oxygen ratios, as noted by others.

Future conceptions of microchannel networks include small separation channels for on-line immunoassay techniques. In many cases, it may be necessary to block the surface of such capillaries to prevent adsorption of these reagents. One effective blocking reagent used for membrane-based immunochromatography is BSA. Therefore, the effect of BSA-coated photoablated polymer surfaces on electroosmotic flow was also studied. After application of the protein solution, the channel was washed by electroosmotic flow pumping by applying an electric field of +250 $V_{dc} \cdot cm^{-1}$ for 10 min. Initial studies showed that, after rewashing the fluid reservoirs and reapplying an electric field, no protein could be detected leaving the microchannel and entering the anodic reservoir, indicating that the protein coating was strongly adsorbed onto the photoablated polymer surfaces. After this washing procedure, the electroosmotic flow was measured as previously described, and the results are displayed in Table 1.

The current monitoring technique was used previously to determine a value of 1.5 $mm \cdot s^{-1}$ for $\nu_{EOF}$ on standard fused silica capillaries with an applied field of 300 $V \cdot cm^{-1}$.[16] This corresponds to a $\mu_{EOF}$ of $5 \times 10^{-4}$ $cm^2 \cdot V^{-1} \cdot s^{-1}$. It can be seen in Table 1 that, for photoablated polymers as a group, $\nu_{EOF}$ and $\mu_{EOF}$ are closely related to those parameters observed on standard fused silica

(17) Lazare, S.; Hoh, P. D.; Baker, J. M.; Srinivasan, R. *J. Am. Chem. Soc.* **1984**, *106*, 4288.
(18) Sroog, C. E. *J. Polym. Sci.* **1976**, *11*, 186.
(19) Chan, C. M.; Ko, T. M. *Surf. Sci. Rep.* **1996**, *24*, 1–54.
(20) Eryu, O.; Yamaoka, K.; Masuda, K. In *Laser Ablation in Materials Processing: Fundamentals and Application*; Braren, B., Dubowski, J. J., Norton, D. P., Eds.; Materials Research Society Symposium Proceedings 285; Materials Research Society: Pittsburgh, PA, 1993; pp 57–61.

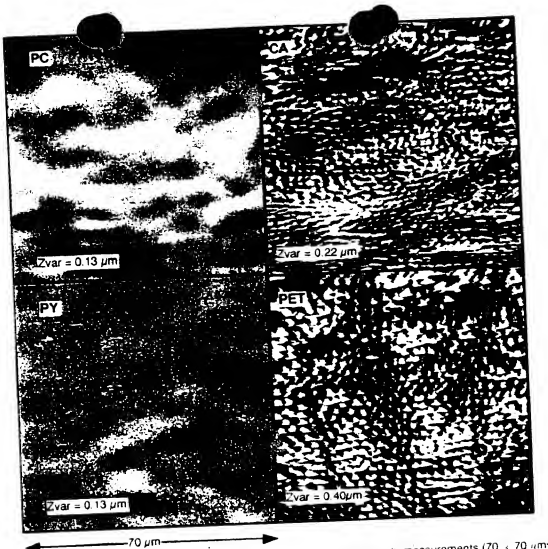


**Figure 4.** Atomic force microscopy of a photoablated polymer surface. AFM surface rugosity measurements (70 × 70 $\mu m^2$ sample section) of (PC) photoablated polycarbonate, (PY) photoablated polystyrene, (CA) photoablated cellulose acetate, and (PET) photoablated polyterephthalate). $Z_{var}$ = average variation ($\mu m$) in surface height

**Table 1. Surface and Electroosmotic Flow Characteristics of Photoablated Polymers with and without Protein Coating**

| substrate | rugosity ($\mu$m) | $\zeta$ potential (mV) | $r_{EOF}$ ($\mu m \cdot s^{-1}$) | $\frac{r_{EOF}}{(E_{cm} \cdot V^{-1} \cdot S^{-1}) \times 10^4}$ |
|---|---|---|---|---|
| unablated polymer | 0.01 | na[a] | na[a] | 1.20 |
| polycarbonate | 0.13 | −52.75 | 0.91 | 2.42 |
| BSA-coated PC | 0.13 | −30.47 | 0.53 | 1.47 |
| polystyrene | 0.13 | −56.22 | 0.97 | 4.47 |
| BSA-coated PY | 0.13 | −35.71 | 0.62 | 2.84 |
| cellulose acetate | 0.27 | −59.65 | 1.03 | 4.74 |
| BSA-coated CA | 0.22 | −29.01 | 0.50 | 2.31 |
| PET | 0.29 | −72.85 | 1.26 | 5.79 |
| BSA-coated PET | 0.4 | −39.83 | 0.69 | 3.17 |

[a] Not applicable.

capillaries. In studies of fused silica capillaries, it has been observed that the $\zeta$ potential is the single most important factor for the characterization of electroosmotic flow. The $\zeta$ potentials for the photoablated polymers studied here were calculated and are shown in Table 1. Others have used the current monitoring method to determine a value of approximately −150 mV for fused silica using similar buffer and field conditions.[1] As a group, the ablated polymers demonstrated $\zeta$ potentials approximately 2−3 times lower than this value. Accordingly, electroosmotic flow, concomitant with CE separations or used as a pump for $\mu$-TAS, will be similar to that for fused silica but slightly smaller in magnitude for photoablated polymer fluid-handling systems. The flow rates determined here certainly demonstrate that UV photoablated polymer microchannels can provide a source of liquid pumping for miniaturized chemical analysis systems.

There were also a number of significant comparisons and contrasts seen between the different photoablated polymers. The overall magnitude of electroosmotic flow followed the series polycarbonate < polystyrene < cellulose acetate < polyterephthalate). An incremental increase in the electroosmotic flow parameters is seen from polycarbonate to cellulose acetate; however, a marked increase in flow was seen with polyterephthalate). It is interesting that this increase in flow also corresponded with the increased surface rugosity seen after ablation. The increased surface area could function to increase the charge density of the functional groups generated by the photoablative process, which would, thereby, increase the $\zeta$ potential and the resulting electroosmotic flow when an electric field is applied. Another non-mutually exclusive possibility is that the increased rugosity might be resulting from a material-specific increased absorption of UV energy. This would include increased bond breaking and increased functionalization of the resulting surface.

**Table 2. Electroosmotic Flow Reproducibility and Repeatability**

| substrate | reproducibility (%) | repeatability (%) |
|---|---|---|
| polycarbonate | 1.81 | 11.18 |
| BSA-coated PC | 2.48 | |
| polystyrene | 1.57 | 3.71 |
| BSA-coated PY | 2.27 | |
| cellulose acetate | 2.14 | 10.06 |
| BSA-coated CA | 2.26 | |
| PET | 2.89 | 9.04 |
| BSA-coated PET | 2.53 | |

Protein coating with BSA was observed to have a significant dampening effect on electroosmotic flow parameters for all of the observed substrates. Across substrates, this reduction was 43.8% for $\nu_{EOF}$. The reduced flow is most probably due to the fact that the BSA is denaturing upon interaction with the charged photoablated surface. This type of surface interaction can often lead to the exposure of hydrophobic regions of the protein, which are normally sequestered in the three-dimensional structure. Therefore, the BSA might be acting to shield much of the charged nature of the photoablated polymer surface and, thereby, reduce the resulting electroosmotic flow.

The reproducibility as well as the repeatability of the electroosmotic flow was determined for the four photoablated polymers, as shown in Table 2. The reproducibility of electroosmotic flow as measured by the current monitoring method ranged from 1.5 to 2.9% within a single microchannel. The repeatability among multiple microchannels ranged from 3.7 to 11.2%. The variation across channels is most likely polymer independent, with the sources of variation principally coming from the correct focusing of the laser on the initial polymer substrate and from the lamination process. For these experiments, we constantly use substrates of varying thickness; therefore, in this research environment, the laser is frequently refocused with some degree of imprecision.

The movement of the negatively charged dye Eosin B (2−) was also studied alongside that of the electroosmotic flow as a function of the applied field. Because the dye is negatively charged, dye electrophoresis will proceed toward the anode. In our experiments, the dye moves toward the cathode because electrophoresis is superimposed on electroosmotic flow, and the electroosmotic flow is in this direction. The velocities of both the electromigration of Eosin B and the electroosmotic flow were observed to be linear in the range of 0−480 $V_{dc} \cdot cm^{-1}$, as shown in Figure 5. Using a relatively low strength buffer (12 mM phosphate buffer, pH 7.0), the total current in the fluid circuit was always less than 10 $\mu$A; therefore, no significant heating effects are expected to have influenced electrophoresis or electroosmotic flow. The $\mu_{EOF}$ across all voltages is (3.98 ± 0.28) × $10^{-4}$ $cm^2 \cdot V^{-1} \cdot s^{-1}$. The small deviation does correspond to a consistent rise along with the applied field, but, as can be seen in Figure 5, this effect does not cause the $\mu_{EOF}$ to deviate from linearity within the range of applied fields tested.

**Effects of Ionic Strength and pH.** It has been well noted in the literature that electroosmotic flow is influenced by the buffer electrolyte concentration due to the effect that ionic strength has on the $\zeta$ potential.[1] It is well known that the higher the ionic strength of the buffer system, the more the double layer is compressed and, therefore, the lower the resulting electroosmotic

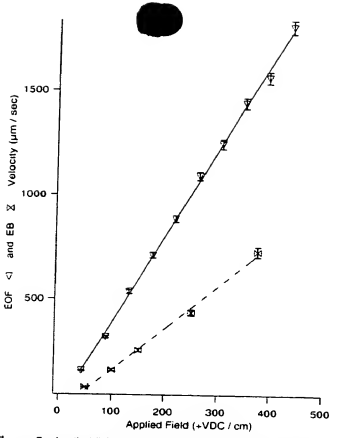


**Figure 5.** Applied field versus linear velocity of electroosmotic flow and the test dye, Eosin B (EB).

flow. This fundamental relationship was expected to be equally applicable to a photoablated polymer surface as it is within fused-silica capillaries; however, as this is the first characterization of electroosmotic flow on photoablated polymers, the absolute magnitude of this effect was important to observe. The ionic concentration of a typical phosphate buffer system was varied according to the total salt concentration (6−100 mM), and the $\nu_{EOF}$ was observed with the current monitoring technique, as shown in Figure 6. As can be seen, a logarithmic response was generated, where $\mu_{EOF}$ was inversely proportional to ionic strength. The overall difference of $\mu_{EOF}$ varied by approximately a factor of 2 over 6−100 mM total salt concentration of a phosphate buffer, pH 7.0.

The pH will also directly alter the charged nature of surface functionalities and thereby change the resulting electroosmotic flow, as described previously for fused silica capillaries.[1] Citrate, phosphate, and borate buffer systems of pH 4, 7, and 10 were used to characterize the response of the photoablated surface to changes in pH/buffer types, as shown in Figure 7. The $\nu_{EOF}$ was observed to dramatically increase with buffer pH, especially in the pH 7−10 region. These experiments indicate a surface with a net negative charge and a $pK_a$ between 4 and 7. As the pH is raised, surface groups are deprotonated, and $\zeta$ is increased. The negatively charged nature of the photoablated surfaces has also been indicated in previous experiments by the direction of the electroosmotic flow, which was observed to be toward the cathode. The response of $\nu_{EOF}$ to applied voltage was linear between +100 and +500 $V_{dc} \cdot cm^{-1}$ for pH 4 and 7; however, the very highest voltage tested at pH 10 begins to show a deviation from this relationship. This region also is correlated with the highest current loads in the fluid circuit, which approached but never exceeded 10 $\mu$A. It is possible that some heating effects and their

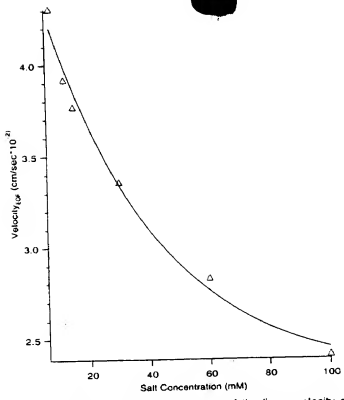


**Figure 6.** Effect of buffer ionic strength of the linear velocity of electroosmotic flow and surface ζ potential on a 40 mm wide polycarbonate microchannel.

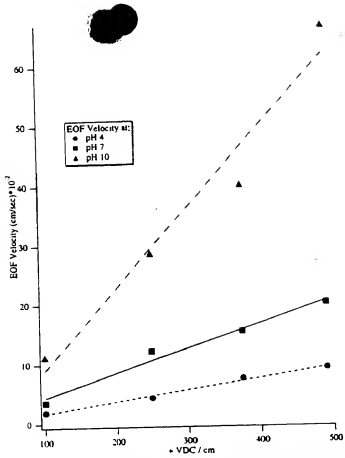


**Figure 7.** Effect of buffer pH on the linear velocity of electroosmotic flow and surface ζ potential on a 40 μm wide polycarbonate microchannel.

concomitant changes in buffer viscosity across the axis of the microchannel are being observed in this region of the testing environment, which are then leading to disproportionate increases in $\nu_{EOF}$.

## CONCLUSIONS

This initial report has described a UV excimer laser-based alternative method for the microfabrication of liquid-handling channels and channel networks, which is capable of producing micrometer-sized features with high aspect ratios. With respect to μ-TAS systems, this method produces structures in novel polymer substrates, which, in the case of polystyrene, polycarbonate, cellulose acetate, and poly(ethylene terephthalate), were shown here to possess negatively charged, functionalized surfaces capable of generating electroosmotic flow in the same direction and on the same order as observed with fused silica capillaries and other μ-TAS devices. The resulting photoablated polymer channels and channel networks could be sealed with a PET/PE laminate at 125 °C in as little as 3 s using a commercially available lamination process. This should offer the possibility for the preapplication/deposition of sensitive biological receptors without extensive thermal degradation.

Many diagnostic and general analysis systems, often referred to as μ-TAS, which could be fabricated using UV laser photoablation require the use of electroosmotic flow as an efficient pump for micro-scale fluid networks. Therefore, as an initial basis for the development of these systems, this report has provided quantitative information on electroosmotic flow parameters as a function of polymer substrate, applied field, buffer ionic strength, and pH.

On-going and future work in our laboratory involving photoablated μ-TAS systems includes the deposition of enzyme-sensing zones inside polymer channels for the detection of substrates of toxicological interest. Massively parallel sampling channels are currently being developed that will connect to these sensing channels. Therefore, future embodiments will include polymer device plates capable of handling multiple samples, which will be subsequently delivered by electroosmotic flow to the sensing channel in an automated manner.

## ACKNOWLEDGMENT

The authors gratefully acknowledge the U.S. National Science Foundation's support for this project with an International Research Fellowship Award to Dr. M. A. Roberts. We also gratefully acknowledge the EPFL and the SPP biotechnology program for financial support through the Funds National Suisse. Dr. Brian Seddon and Dr. Murray Osborne are thanked for their editorial input and for insightful discussions in the area of developing diagnostic systems.

Received for review October 9, 1996. Accepted March 4, 1997.[*]

AC961038Q

[*] Abstract published in *Advance ACS Abstracts*, April 15, 1997.